Mobility and Engineering Research (MER)
Volume 1/2018

A computational tool for investigations on the lifetime estimation of multi-directional laminates under multiaxial stress states based on layerwise structural analysis

Marc Möller, Jochen Blaurock, Gerhard Ziegmann, Alfons Esderts

Technology
Arts Sciences
TH Köln

A computational tool for investigations on the lifetime estimation of multi-directional laminates under multiaxial stress states based on layerwise structural analysis

Marc Möller[a,*], Jochen Blaurock[a], Gerhard Ziegmann[b], Alfons Esderts[c]

[a] *Institute for Automotive Engineering, TH Köln, Betzdorfer Straße 2, 50679 Cologne, Germany*
[b] *Institute of Polymer Materials and Plastics Engineering, TU Clausthal, Agricolastraße 6, 38678 Clausthal-Zellerfeld, Germany*
[c] *Institute for Plant Engineering and Fatigue Analysis, TU Clausthal, Leibnizstraße 32, 38678 Clausthal-Zellerfeld, Germany*

Abstract

In the present paper a calculation tool for the lifetime prediction of composite materials with focus on local multiaxial stress states and different local stress ratios within each lamina is developed. The approach is based on repetitiv, progressive in-plane stress calculations using classical laminate theory with subsequent analysis of the material stressing effort and use of appropriate material degradation models. Therefore experimentally data of S-N curves are used to generate anistropic constant life diagrams for a closer examination of critical fracture planes under any given combination of local stress ratios. The model is verified against various balanced angle plies and multi-directional laminates with arbitrary stacking sequences and varying stress ratios throughout the analysis. Different sections of the model, such as residual strength and residual stiffness, are examined and verified over a wide range of load cycles. The obtained results agree very well with the analyzed experimental data.

Keywords: Composite, Multiaxial fatigue, Lifetime prediction, Multi-directional Laminate, Plywise modeling

1. Introduction

The growing awareness of climate change and its recognition in many different economic sectors and, associated therewith, the increasing need of strong lightweight materials makes the use of composites become more and more important over a wide range of structural parts. Thus there is a strong demand for efficient design and the continuous improvement of material utilization in the field of fibre-reinforced plastics (FRP). During operation, most structural components are subjected to multiaxial and cycling loads, which make a closer look to the fatigue material behavior of composites even more necessary. To estimate the lifetime of various fibre-reinforced plastic laminates, with arbitrary stacking sequences under complex multiaxial stress states, a mathematical tool based on plywise-modelling is developed. The phenomenological comparability between progressive material failure due to quasi-static loads and failure due to fatigue loads, is the reason why the model is based on extending the classical laminate theory (CLT) to fatigue loads. Extensive research in the field of composite fatigue has been carried out, but, as described in section 2, there is no overall approach or tool for investigations on multiaxial fatigue loads and only few laminates have been previously examined in mechanistic models under mostly only tension-tension loads. To provide an instrument for further investigations on modeling fatigue material behavior of several layups under varying load conditions, different isolated state-of-the-art models are considered and put together in a computational tool written in python. The developed model consists of multiple individual elements, such as formulation of S-N curves, the way of interpolating between stress ratios via constant life diagrams, choice of (quasi-static) failure criteria, formulations for embedded lamina, a concept of shrinking failure envelope due to different combinations of transverse and shear stress ratios and of course stiffness as well as strength degradation models. Considering the level of complexity and the amount of individual concerns within the model, it

*Corresponding author
Email addresses: marc.moeller@th-koeln.de (Marc Möller), jochen.blaurock@th-koeln.de (Jochen Blaurock), ziegmann@puk.tu-clausthal.de (Gerhard Ziegmann), alfons.esderts@imab.tu-clausthal.de (Alfons Esderts)

Nomenclature				
$E_{\parallel}$	$(\hat{E}_1)$	Elastic modulus in $\parallel$ (1) - direction	$\hat{\sigma}_m$	Global mean stress of laminate
$E_{\perp}$	$(\hat{E}_2)$	Elastic modulus in $\perp$ (2) - direction	$\hat{\sigma}_a$	Global stress amplitude of laminate
$G_{\perp\parallel}$	$(\hat{G}_{12})$	In plane shear modulus	$\sigma_{\parallel m}, \sigma_{\perp m}, \tau_{\perp\parallel m}$	Lamina mean stresses
$\nu_{\perp\parallel}$	$(\hat{\nu}_{21})$	Major Poisson's ratio	$\sigma_{\parallel a}, \sigma_{\perp a}, \tau_{\perp\parallel a}$	Lamina stress amplitudes
$\nu_{\parallel\perp}$	$(\hat{\nu}_{12})$	Minor Poisson's ratio	$R_{\sigma_{\parallel}}$	Stress ratio of $\sigma_{\parallel}$ - stresses
$\nu_{f\perp\parallel}$		Major Poisson's ratio of fibre	$R_{\sigma_{\perp}}$	Stress ratio of $\sigma_{\perp}$- stresses
$E_{f\parallel}$		Parallel elastic modulus of fibre	$R_{\tau_{\perp\parallel}}$	Stress ratio of $\tau_{\perp\parallel}$- stresses
$m_{\sigma f}$		Magnification factor	R	Stress ratio of global stresses
φ		Fibre volume fraction	$\overline{Q}_{ij}$ (Q_{ij})	Lamina(te) stiffness matrix
$\sigma_{\parallel}$	$(\hat{\sigma}_1)$	Normal stress in $\parallel$ (1) - direction	A_{ij}	Shell stiffness matrix
$\sigma_{\perp}$	$(\hat{\sigma}_2)$	Normal stress in $\perp$ (2) - direction	B_{ij}	Shell-plate interaction matrix
$\tau_{\perp\parallel}$	$(\hat{\tau}_{21})$	In-plane shear stress	D_{ij}	Plate stiffness matrix
X_t	$(\hat{X}_t)$	Parallel tension strength	f_e	Stress exposure factor
X_c	$(\hat{X}_c)$	Parallel compression strength	f_w	Weakening factor for influence of $\sigma_{\parallel}$
Y_t	$(\hat{Y}_t)$	Transverse tension strength	$p^+_{\perp\parallel}, p^-_{\perp\parallel}$	Incline of failure envelope at $\sigma_{\perp} = 0$: „+ “ for $\sigma_{\perp} > 0$ and „- “ for $\sigma_{\perp} < 0$
$Y_t^{'}$		(In-situ) Transverse tension strength of embedded lamina	$p^+_{\perp\perp}, p^-_{\perp\perp}$	Incline of failure envelope at $\sigma_n = 0$: „+ “ for $\sigma_{\perp} > 0$ and „- “ for $\sigma_{\perp} < 0$
Y_c	$(\hat{Y}_c)$	Transverse compression strength	$R^A_{\perp\perp}$	Fracture resistance due to $\tau_{\perp\perp}$
$S_{\perp\parallel}$	$(\hat{S}_{21})$	In plane Shear strength	n_x, n_y, n_{yx}	Internal line forces
$S^{'}_{\perp\parallel}$		(In-situ) In plane Shear strength of embedded lamina	m_x, m_y, m_{yx}	Internal line moments

Table 1: Nomenclatur for most important symbols in lamina coordinate system related to the principal material axis of the unidirectional lamina ($\parallel$, $\perp$, $\perp$) and in brackets for symbols in laminate coordinate system related to the principal material axis of the laminate (1,2,3)

becomes apparent that a lot of coherent experimental data is needed. Because of the lack of own data at that time, the model is validated by comparing the results with experimental data from the well known Composite Material Fatigue Database of the Michigan State University - Department of Energy in cooperation with Sandia National Laboratories (SNL/DOE/MSU - Database) [1] for first investigations.

2. A brief review of progressive and iterative fatigue models for composites

The basic idea in terms of a fatigue-extended classical laminate theory is nothing new and has already been propagated before in differing ways. In 2000, Shokrieh and Lessard [2] proposed a progressive model based on the fatigue failure criterion by Hashin [3] and degradation rules for gradual and sudden change in material properties. They verified the model with experimental data of symmetric graphite/epoxy angle-ply laminates ($[90_4/0_4]_s$,$[0_4/90_4]_s$ and $[+45_4/-45_4]_s$) under tension-tension loads with constant stress ratio R=0.1 [4]. After the onset of a certain failure mode the specific stiffness- and strength entries were set to zero, while gradual degradation is modeled before any failure occurs. Shokrieh and Lessard also discussed the shortcoming of the Miner's rule for calculations with more than one block load for the $[+45_4/-45_4]_s$-laminate. For the constant block loading the model achieved good results for the fatigue life. Noll, Magin and Himmel [5] examined, in particular, the effect of a nonlinear shear stress-strain ($\tau\perp\parallel$, $\gamma_{\perp\parallel}$) - relation within a progressive composite fatigue model and the use of the critical element concept. They used the failure criterion by Puck[6] and a stiffness degradation model, which reduces some entries in the stiffness matrix to a certain value after the onset of a specific failure. Their model was verified calculating the fatigue life of a vinylester/urethane/carbon quasi-isotropic composite laminate ($[45/0/-45/90]_s$) under variable amplitude loading with constant stress ratio R=0.1. The comparison with experimental data showed that the use of linear stress-strain behavior and ignoring stiffness degradation led to overestimation of fatigue life for the examined laminate. Kennedy, Bradaigh and Leen [7] developed an advanced model with the use of Puck's failure criteria and the s-shaped damage model by Mao and Mahadevan [8] to model stiffness degradation in fibre direction for a unit cell model within a finite element subroutine. Results were examined for a quasi-isotropic (QI)

e-glass/epoxy laminate ($[0/90/45/135]_s$) under tension-tension loads with constant stress ratio R=0.1. The model by Kennedy et al. was seen to predict the fatigue life of the QI-Laminate under R=0.1 very accurately.
In 2016, Neumeister et al. [9] presented a model for multi-directional laminates, which is based on the failure mode concept-based strength criteria by Cuntze [10] and calculation of total damage with a linear damage accumulation model. The stiffness degradation follows a nonlinear behavior, which is related to the calculated damage, based on [11]. Neumeister et al. presented first results of the simulation for a $[\pm 45/90]_s$-laminate, but the model itself was not verified to any experimental data within the publication.
In 2017, Mejlej, Osorio and Vietor [12] proposed a progressive model for multi-directional laminates under varying stress ratios. The model is build upon the total energy based model by Shokrieh [13], the use of Hashin Failure Criteria and the gradual stiffness degradation by Shokrieh and Lessard [2]. Mejlej et al. applied a relation of fatigue life and total input energy, which is based on fitting parameter to a set of S-N curves, regardless to the stress ratio and fibre orientation. They used the energy failure criterion from Sandhu [14] to calculate fatigue life for various fibre angles and stress ratios. The model was verified against two sets of unidirectional ($[0]_{12}$) laminate made of carbon/epoxy under both positive and negative stress ratio. The calculation of fatigue life conforms very well to the experimental data under varying stress ratios for unidirectional material.
Finally the methodology and tool developed by Vassilopoulos et al. [15] for GFRP lamiantes under complex stress states is briefly mentioned, although it does not really belong to the iterative models. The model uses cycle counting methods for spectrum loads, different fatigue criteria for life prediction, such as e.g. the Fawaz-Ellyin [16] or Hashin-Rotem Criterion [17], and the linear Miner rule for damage summation. The model gets along without the use of stiffness or strength degradation, since it calculates allowable numbers of cycles for each block directly using the mentioned fatigue failure criteria. Differing designs of S-N curves and constant-life-diagrams were examined within the model. Verification was carried out for variable amplitude loading on e-glass/polyester laminates ($[0/(\pm 45)_2/0]_s$) for alternating and pulsating stress ratios, focusing mainly on the comparison of used fatigue failure criteria.
In short, there are quite a few models for different aspects of fatigue life of composites available. The above mentioned models are based on progressive modeling and vary widely in e.g. used failure criteria or in the way of describing material degradation of strength and stiffness.

For future research in multiple segments of composite fatigue, a general model is presented below and a calculation tool called „**L**ifetime **E**stimation **o**f **C**omposites“ (LEoC - Fig. 1) is developed using the programming language „Python“.

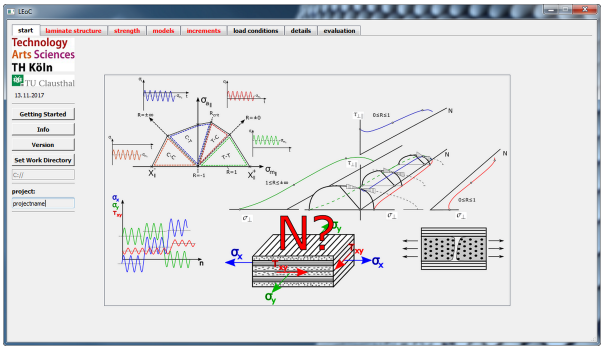

Fig. 1: Startup-screen of „LEoC“ for investigations on fatigue of composite

3. Tool and Flow chart for fatigue failure analysis

The simulations are performed on the lamina level using a representative volume element (RVE) of the laminate, which represents the corresponding mechanical properties of a structural part or component as visualized in Fig. 2. Load conditions in terms of internal line forces and moments are applied to the RVE. The general program

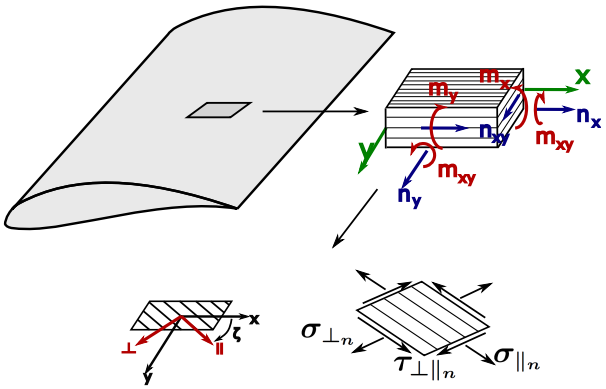

Fig. 2: Simulation of 2-D (plane stress) representative volume element (RVE) of exemplary structural component on the lamina level (meso-scale)

schedule is demonstrated in Fig. 3, without mentioning which specific models are applied at particular points in the code. The reason for this is that, in principle, diverse models can possibly be applied at every main subject. The divisions along the dashed lines in Fig. 3, which are

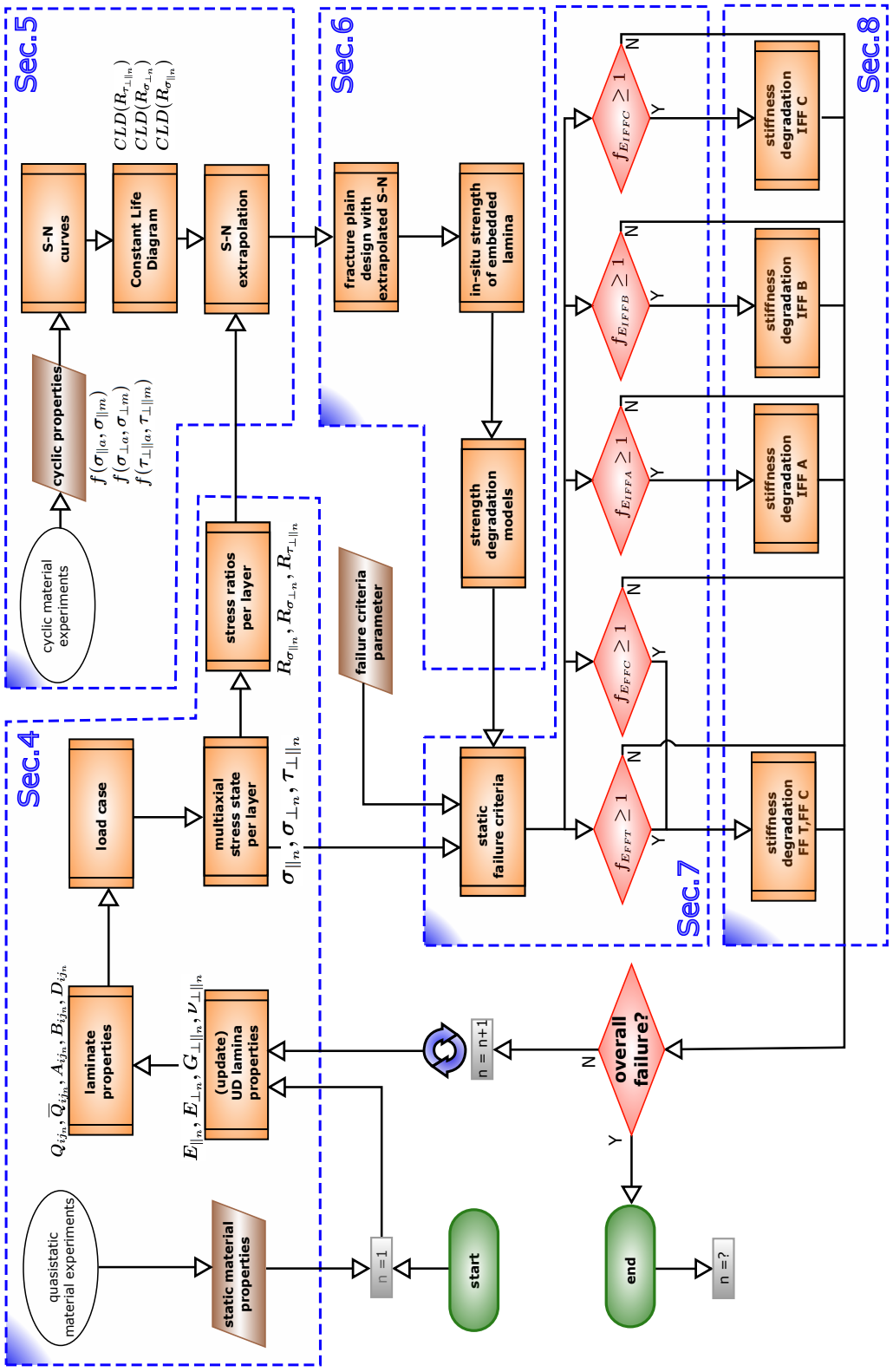

Fig. 3: flow chart for the lifetime estimation of fibre reinforced composites within LEoC

labeled from „Sec. 4“ until „Sec. 8“, represent the following sections and the examined areas of focus within this paper:

- In section 4, the necessary data from quasi-static material tests for initial conditions of laminate properties is discussed.
- Furthermore, input needed from cycling material tests and the design of constant life diagrams, for the extrapolation of unknown S-N curves at arbitrary stress ratios, is explained in section 5.
- Using the extrapolated S-N curves, the following strength degradation according to the current multiaxial stress state is addressed in section 6.
- In section 7, the failure analysis is considered and the choice of used failure criteria justified.
- Models for stiffness degradation after the onset of specific failure modes are discussed and applied to the model in section 8.

The failure condition with its different types of failure on the ply-level, as explained in section 7, is checked for every layer in the current load cycle and as far as failure did not occur in every existing ply, the next load cycle is applied to the current laminate condition. The iterative process is carried on until the laminate failed in every ply or the number of intended load cycles is reached.

4. Input from quasi-static material tests

One of the decisive initial conditions in these calculations are the static stiffness and strength properties at the ply-level as demonstrated in Fig.3 - field section number 1. Necessary input data of material „D155“ (Fibre: Glass fabric -527 g/m^2, Matrix: Orthophthalic Polyester „CoRezyn 63-AX-051“) from [1] is exemplarily shown in table 2. The initial state of the laminate in every cycle n is derived using the CLT. The stiffness matrix of each lamina „k“ in the lamina (local) coordinate system is obtained by

$$Q_{ij,k}(n) = \begin{bmatrix} \dfrac{E_\parallel(n)}{1-\Delta(n)} & \dfrac{\nu_{\perp\parallel}(n)E_\parallel(n)}{1-\Delta(n)} & 0 \\ & \dfrac{E_\perp(n)}{1-\Delta(n)} & 0 \\ (sym.) & & G_{\perp\parallel}(n) \end{bmatrix} \quad (1)$$

with $\Delta(n) = \nu_{\perp\parallel}(n)\nu_{\parallel\perp}(n)$ and experimental data from quasi-static material tests, as shown in table 2. The reduced stiffness matrix of each lamina in the global coordinate system is calculated by

$$\overline{Q}^{\pm\xi}_{ij,k}(n) = T_{ij}Q_{ij,k}(n)T_{ji} \quad (2)$$

	$E_\parallel$ $[GPa]$	$E_\perp$ $[GPa]$	$G_{\perp\parallel}$ $[GPa]$	$\nu_{\perp\parallel}$ $[-]$	
$\overline{x}$	33.60	8.21	4.48	0.29	
s	1.80	0.72	1.11	0.01	
$\overline{\varphi}$	0.44	0.44	0.40	0.44	
	X_t $[MPa]$	X_c $[MPa]$	Y_t $[MPa]$	Y_c $[MPa]$	$S_{\perp\parallel}$ $[MPa]$
$\overline{x}$	1012.0	653.0	27.00	122.75	73.2
s	29.0	23.3	1.63	9.91	5.8
$\overline{\varphi}$	0.44	0.41	0.44	0.44	0.44

Table 2: Exemplary static values ($\overline{x}$: arithmetic mean, s: standard deviation and $\overline{\varphi}$: mean fibre volume fraction) used for simulation input from experimental data of material D155 [1]

with use of the transformation matrix

$$T_{ij} = \begin{bmatrix} cos^2(\xi) & sin^2(\xi) & -sin(2\xi) \\ sin^2(\xi) & cos^2(\xi) & sin(2\xi) \\ 0.5sin(2\xi) & -0.5sin(2\xi) & cos(2\xi) \end{bmatrix} .$$

The overall global distortions of the laminate are given by:

$$\underline{\hat{\epsilon}}_k(n) = \hat{\epsilon}_i^{'}(n) + z \cdot \underline{\hat{\kappa}}^{'}(n) \quad (3)$$

Herein the distortions are calculated using the strains and curvatures of the combined shell and plate element, which are obtained from

$$\begin{pmatrix} \hat{\epsilon}_i^{'}(n) \\ \hat{\kappa}_i^{'}(n) \end{pmatrix} = \begin{bmatrix} A^*_{ij}(n) & B^*_{ij}(n) \\ (B^*_{ij}(n))^T & D^*_{ij}(n) \end{bmatrix} \cdot \begin{pmatrix} \hat{n}_{i,bl} \\ \hat{m}_{i,bl} \end{pmatrix} \quad (4)$$

where $\hat{n}_{i,bl} = \{n_x, n_y, n_{xy}\}$ and $\hat{m}_{i,bl} = \{m_x, m_y, m_{xy}\}$ are the internal line forces and moments of the current block load, as shown in Fig. 2. The extensional- (A^*_{ij}), bending- (D^*_{ij}) and coupling- (B^*_{ij}) compliance matrices are calculated by inverting the ABD matrix with the use of the respective stiffness matrices:

$$\frac{1}{\chi}\sum_{k=1}^{n}\overline{Q}_{ij,k}\left(z_k^\chi - z_{k-1}^\chi\right) = \begin{cases} A_{ij}, & \text{for } \chi = 1 \\ B_{ij}, & \text{for } \chi = 2 \\ D_{ij}, & \text{for } \chi = 3 \end{cases} \quad (5)$$

The global distortions and the transformed stiffness matrix are then used to calculate the global stress vector for each lamina. The local in-plane stresses are calculated subsequently with the use of the transformation matrix.

$$\hat{\sigma}_{i,k}(n) = \overline{Q}_{ij,k}(n) \cdot \hat{\epsilon}_{i,k}(n) \quad (6)$$

$$\sigma_{i,k}(n) = T_{ij}\hat{\sigma}_{i,k}(n) \quad (7)$$

where $\sigma_{i,k}(n)$ is the local stress vector, with the entries $\sigma_{\parallel,k}(n)$, $\sigma_{\perp,k}(n)$ and $\tau_{\perp\parallel,k}(n)$ for each ply number k.

5. Input from fatigue material tests

Stress calculations (equation 7) are carried out for two different sets of load conditions $\hat{n}_{i,bl}$ and $\hat{m}_{i,bl}$ in every block load to gain the multiaxial stress ratios $R_{\sigma_\parallel}, R_{\sigma_\perp}, R_{\tau_{\perp\parallel}}$ for all three present stress components $\sigma_\parallel, \sigma_\perp, \tau_{\perp\parallel}$. The present work will focus mainly on simulations with stress ratios in pulsating tension ($0 \leq R < 1$) and pulsating compression range ($1 < R \leq \infty$), as shown in Fig. 4. In the following the four sectors of stress ratio ranges will be referred to as:

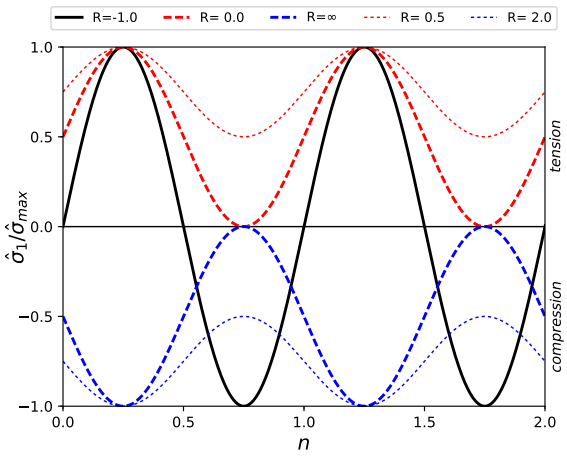

Fig. 4: Cyclic stresses for one alternating stress ratio (R=-1) and in each case two pulsating tension (R=0, R=0.5) and pulsating compression (R=−∞, R=2) stress ratios

- T-T: Tension-tension pulsating range ($0 \leq R < 1$)
- T-C: Tension dominated alternating range ($-1 \leq R < 0$)
- C-T: Compression dominated alternating range ($-\infty \leq R < -1$)
- C-C: Compression-compression pulsating range ($1 < R \leq \infty$)

Required relations between stress and endured cycles in terms of S-N curves are obtained by fitting experimental data to the logarithmic linear relation by Basquin:

$$N = C \cdot \sigma_a^{-k} \tag{8}$$

where N is the number of cycles, C is the Y intercept, k is the negative slope and σ_a is the stress amplitude of the current block load for each of the three stress components from equation 7. S-N curves at stress ratio R=0.1 (representative for R=0) and R=10 (representative for R=∞) are at least required to interpolate data at arbitrary stress ratios in pulsating tension-tension and compression-compression range. Fig. 5 exemplarily shows the fitted S-N curves for experimental data of material „D155“ from [1].

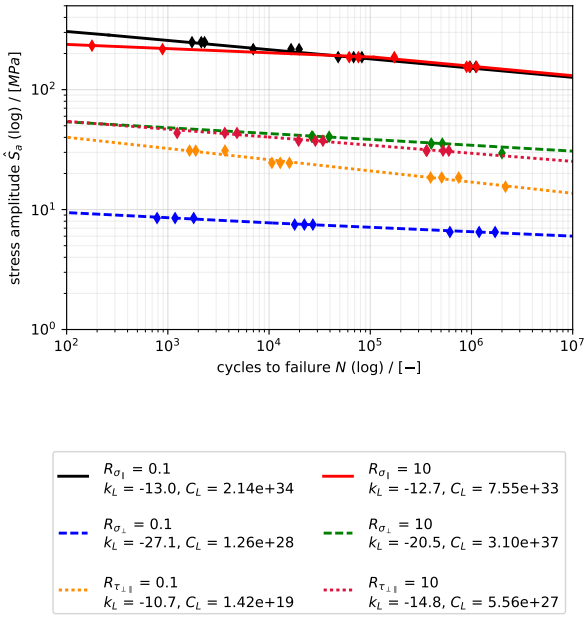

Fig. 5: Least required S-N curves for investigations in pulsating tension and compression range with experimental data for unidirectional Material D155 [1]

One way to receive unknown S-N curves at other stress ratios is by using constant life diagrams (CLD), also often referred to as Haigh-, Goodman- or Smith-Diagrams. A historical view on the development of CLD can be found in [18]. For multiaxial stress states of the lamina, three independent constant life diagrams for parallel, transverse and shear properties are necessary.

A comprehensive investigation on the influence of different formulations of CLD for a limited number of multidirectional glass/polyester laminates has been carried out by [19]. The linear model, which is based on using only one experimental S-N curve, at e.g. stress ratio $R = -1$, underestimates the strength of the materials in almost all cases for any stress ratio and leads to extremely conservative results. Still it is often used, e.g. in wind turbine certification [20] for the fatigue of FRP, or simply because of the lack of data. The nonlinear fatigue life diagram by Kawai [21], the parametric constant-life model by Harris [22], the multislope model by Boerstra [23] and the piecewise linear (PWL) model by Philippidis and

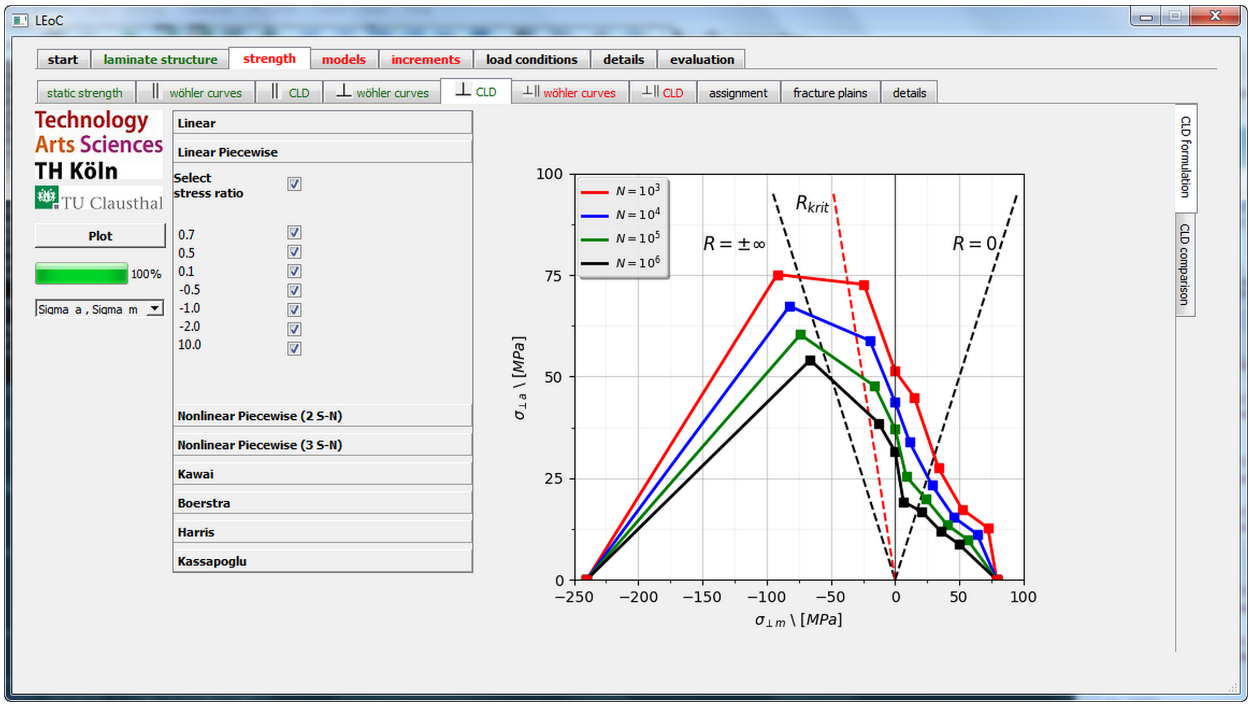

Fig. 6: Exemplary construction of transverse piecewise linear (left) and piecewise nonlinear (right) constant life diagram in LEoC for experimental data from [1]

Vassilopoulos [24] showed to give very accurate results for most of the examined fatigue data. Vassilopoulos et. al especially pointed out the sensitivity of Kawai's model to the choice of input data and the sensitivity of the models by Boerstra and Harris to the fitting of model parameters. Furthermore the model by Kawai tends to often lead to overestimation of the material and therefore non-conservative results. Of all of these models, the PNL seems to be the most stable, since it depicts the S-N behavior by linear interpolation between known S-N curves without any preliminary assumptions. Vassilopoulos et al. also improved their formulation in terms of a piecewise nonlinear (PNL) constant life diagram formulation [25] based on the use of two (PNL-2R) or three (PNL-3R) S-N curves. The accuracy of the nonlinear formulation was very considerable for the same examined data as in [19].

Nonetheless, in the present work the piecewise linear (PWL) model by Philippidis and Vassilopoulos [24] will be preferably used for first investigations on fatigue life (see Fig. 6). Of course, the PNL proves to be only very accurate for a reasonable amount of known S-N curves (at least three S-N curves, each one preferably at the border of every sector (T-T/T-C, T-C/C-T and C-T/C-C). Thus, at least three S-N curves at stress ratios R=0.1, R=-1 and R=10 are most commonly used for a separation into four sectors . Thus, for the design of three piecewise linear CLD a designated number of S-N curves and the static compression and tension strengths in parallel, transverse and shear direction (X_t, X_c, Y_t, Y_c and $S_{\perp\parallel}$) are needed.

The calculation of stress amplitude σ_a^* at R^*, if R^* is in between R=1 and the first known stress ratio moving counter clockwise ($R_{1,ccw}$), is defined as follows:

$$\sigma_a^* = \frac{X_t}{\frac{X_t}{\sigma_{a,1,ccw}} + r^* - \frac{(1+R_{1,ccw})}{(1-R_{1,ccw})}} \tag{9}$$

with $\sigma_{a,1}$ being the stress amplitude at $R_{1,ccw}$ and $r^* = (1+R^*)/(1-R^*)$. If R^* is in between R=1 and the first known stress ratio moving clockwise ($R_{1,cw}$):

$$\sigma_a^* = \frac{X_c}{\frac{X_c}{\sigma_{a,1,cw}} + r^* - \frac{(1+R_{1,cw})}{(1-R_{1,cw})}} \tag{10}$$

where $\sigma_{a,1}$ is the stress amplitude at $R_{1,cw}$. If R^* is located in between any of two used stress ratios R_i and R_{i+1}:

$$\sigma_a^* = \frac{\sigma_{a,i}(r_i - r_{i+1})}{(r_i - r^*)\frac{\sigma_{a,i}}{\sigma_{a,i+1}} + (r^* - r_{i+1})} \tag{11}$$

where $\sigma_{a,i}$ and $\sigma_{a,i+1}$ are the stress amplitudes at the two known stress ratios and $r_{i(i+1)} = (1+R_{i(i+1)})/(1-R_{i(i+1)})$. Fig. 7 shows the piecewise linear constant life formulation for a multi-directional laminate with stacking sequence $[90/0/\pm45/0]_s$. Three S-N curves at stress ratios R=0.1, R=-1 and R=10 are used for linear interpolation, and another three S-N curves at stress ratios R=0.8, R=0.5 and R=2 are plotted for comparison purposes.

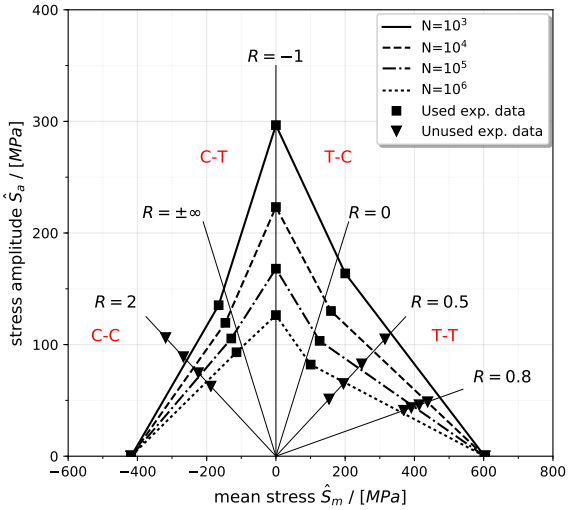

Fig. 7: PWL constant life diagram for laminate „DD16“ with stacking sequence $[90/0/\pm45/0]_s$ from [1]

6. Strength degradation

First of all, there are possibly two ways to do justice to the degradation of strength in laminates: linking the decrease in strength to a physical meaning like micro mechanical damage, e.g. (inter-)fibre failure, or on the other hand connecting it to the number of cycles endured. A large number of residual strength models have already been proposed. Most of the state-of-the-art models have been examined by Philippidis and Passipoularidis [26]. A common way to model the residual strength is the use of S-N curves to set a loss in strength and the actual number of endured cycles as well as the sustainable number of cycles into a certain relation. To begin with, the loss in strength in each step is defined as

$$S_{r,i} = S_{r,i-1} - \Delta S_{r,i} \tag{12}$$

where $S_{r,i}$ and $S_{r,i-1}$ represent the five residual strengths $\{X_t, X_c, Y_t, Y_c, S_{\perp\parallel}\}$ at the actual and the last step respectively. $\Delta S_{r,i}$ is the drop of residual strength in the i-th cycle and is calculated from

$$\Delta S_{r,i} = \left\{ \left[\left(S_{st} - \sigma_{max,i}\right) \left(1 - \left(\frac{n_{i-1}}{N_i}\right)^{\alpha_j}\right)^{\beta_j} \right] - \left[\left(S_{st} - \sigma_{max,i}\right) \left(1 - \left(\frac{n_i}{N_i}\right)^{\alpha_j}\right)^{\beta_j} \right] \right\} \tag{13}$$

where S_{st} is the specific static strength, $\sigma_{max,i}$ is the maximum stress of the ith cycle, n_i and n_{i-1} are the number of cycles at the actual and the last step, N_i is the maximum number of cycles and α_j and β_j are material parameters given by curve fitting of residual strength data.

By varying values of α_j and β_j different material behavior can be achieved. With α_j and β_j being both zero, there won't be any strength degradation of the addressed strength. For $\alpha_j = 1$ and $\beta_j = 1$ equation 12 and 13 can be rearranged to the mostly used linear degradation rule by Broutman and Sahu [27]. Almost all present calculations of residual strength under fatigue loads use the linear model and it is well known that it gives conservative results on the safe side. For arbitrary values of α_j with $\beta_j = 1$ the model represents the nonlinear one-parameter model by Schaff and Davidson [28]. The strength degradation is then simulated with either a steep loss of strength at the beginning (“Rapid initial loss in strength“) or at the end (“Sudden death“) of the laminate lifetime. For all other values of α_j and β_j the equation refers to the „normalized residual strength model (NRSM)“ by Stojkovic et al. [29]. The advantage of the NRSM model is that the typical initial loss of strength followed by slow degradation as well as the sudden decrease in strength at the end can be modeled very well.

For the iterative calculation of residual strength within the subroutine, the strength degradation of every ply needs to be defined. For the case of a three piecewise CLD, there are only theoretical 40 parameters eligible in LEoC to overcome all five strength parameters within every sector of the constant life diagram. This of course makes little sense for a practical application. Thus, linking a few comparable degradation behaviors might be an advantage in reducing the amount of experimental data needed. Since the present work focuses only on pulsating stresses, the amount of data is considerably reduced anyway. Particularly because of the lack of experimental data of unidirectional lamina for material used from [1], the linear degradation of all five strength parameters will preferably be used for calculations of fatigue life. Nonetheless, results for all presented residual strength models will be discussed in section 10. Fig. 8 demonstrates the

use of equation 13 for a multi-directional laminate with stacking sequence $[90/0/\pm45/0]_s$.

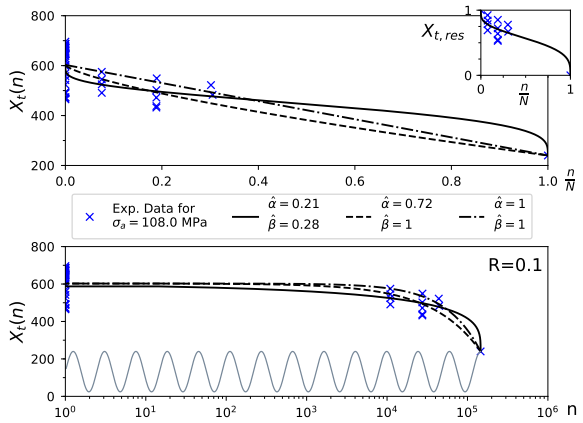

Fig. 8: Comparison of linear, 1 parameter and 2 parameter formulation to residual strength data for $[90/0/\pm45/0]_s$ laminate „DD16“ from [1]

For example, for a constant amplitude $\hat{\sigma}_a = 108$ Mpa and stress ratio R=0.1 residual strength the data at 7.5 %, 19% and 30 % life fraction is available for the MD laminate „DD16“. The upper graph in Fig. 8 shows the residual tensile strength plotted against the life fraction. The reserve factor of $X_{t,res}$ is also shown in the upper right-hand corner, for a better visualization of the two-parameter formulation. The lower semi-logarithmic plot in Fig. 8 illustrates the degradation behavior of a laminate plotted against the number of endured cycles. It is evident that the two-parameter fitted equation by Stojkovic et al. accurately depicts the initial loss of the laminate at the relatively early life stage. Yet, there is no large difference observed until 30 % of life for the examined laminate and the linear- and one-parameter model also capture the residual strength very well to this point. The five measured strength parameters are obtained from experiments with isolated lamina. To do justice to the increase of transverse tensile (Y_t) and in-plane shear strength ($S_{\perp\parallel}$) when being embedded in a laminate, the in-situ formulation by Wang and Karihaloo [30] is used:

$$Y_t^{'} = Y_t \left[1 + \frac{A}{N^B} f_t\left(\Delta\Theta\right) \right], \tag{14}$$

$$S_{\perp\parallel}^{'} = S_{\perp\parallel} \left[1 + \frac{C}{N^D} f_t\left(\Delta\Theta\right) \right] \tag{15}$$

where $Y_t^{'}$ and $S_{\perp\parallel}^{'}$ are the increased transverse tensile strength and in-plane shear strength, $\{A, B, C, D\}$ are material parameters, N is the number of plies of a given thickness in the unidirectional embedded lamina and $f_t\left(\Delta\Theta\right)$ is given by

$$f_t(\Delta\Theta) = min\left[\frac{\sin^2(\Delta\Theta_a)}{1+\sin^2(\Delta\Theta_a)}, \frac{\sin^2(\Delta\Theta_b)}{1+\sin^2(\Delta\Theta_b)} \right] \tag{16}$$

$$f_s(\Delta\Theta) = min\left[\frac{\sin^2(\Delta 2\Theta_a)}{1+\sin^2(\Delta 2\Theta_a)}, \frac{\sin^2(\Delta 2\Theta_b)}{1+\sin^2(\Delta 2\Theta_b)} \right] \tag{17}$$

where $\Delta\Theta_b$ and $\Delta\Theta_b$ are the ply angle differences of both adjacent plies. The increased transverse tensile ($Y_t^{'}$) and in-plane shear strength ($S_{\perp\parallel}^{'}$) are both used in the failure criteria formulation, as Dong et al. [31] already have stated the benefits of improving Puck's failure theory with the in-situ formulation.

7. Failure Criteria

The prediction of static failure strengths of fibre reinforced plastic laminates received massive attention over the last decades and a wide range of various failure criteria have been developed. Within the World-Wide Failure Exercise (WWFE) [32] nineteen different failure criteria have been examined over twelve years to establish the current status of theories for predicting static failure of laminates under several multiaxial stress states. The exercise provides strength and weaknesses in predicting strength and deformation of specimen in various test cases for a lot of the leading theories [33]. Nonetheless the results of the WWFE clearly show that there is no all-encompassing solution for arbitrary multi-directional laminates even in static analyses [34].
The approach for the lifetime estimation of laminates, as presented in Fig.3 - field section number 7, can generally be based on any static failure criteria, which distinguishes between fibre- and matrix failure. Thus a lot of different models can possibly be implemented into the routine. Since the present paper mainly aims to demonstrate the procedure in general, only the failure criteria by Puck [6] is used for first investigations. This can be reasoned with the fact, that Puck's failure criteria performed very well for most of the experimental results in the WWFE and was awarded with the highest number of Grade A's (64/125)[1] of all participating theories. Therefore the use of the failure criteria by Puck seems to be a good choice for initial examinations. One benefit of Puck's failure criteria is the very detailed subdivision into three concurrent matrix failures. In Fig. 9 the sectioning into the failure modes due to transverse tension

[1] Grade A was awarded, if the prediction lies within ± 10 % of the experimental value [32]

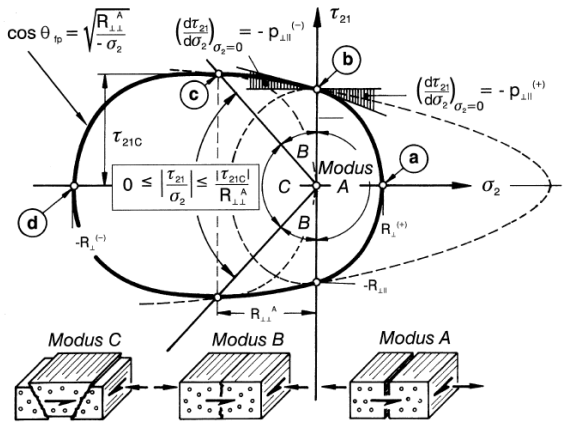

Fig. 9: Failure envelope at $\sigma_{\parallel} = 0$ [6]

stress (Modus A), low transverse compression and high shear stress (Modus B) and high transverse compression and low shear stress (Modus C) on the $\sigma_{\perp}, \tau_{\perp\parallel}$-plane ($\sigma_{\parallel} = 0$) is shown. The inter fibre failure f_e of the unidirectional lamina due to transverse tension (Modus A) within the validity range: $\sigma_{\perp}(n) > 0$ is described according to

$$\sqrt{\left(\frac{\tau_{\perp\parallel}(n)}{S'_{\perp\parallel}(n)}\right)^2 + \left(1 - p^{+}_{\perp\parallel}\frac{Y'_t(n)}{S'_{\perp\parallel}(n)}\right)^2\left(\frac{\sigma_{\perp}(n)}{Y'_t(n)}\right)^2} + p^{+}_{\perp\parallel}\frac{\sigma_{\perp}(n)}{S'_{\perp\parallel}(n)} = f_{e,IFFA}(n) \tag{18}$$

The inter fibre failure f_e for Modus B for $\sigma_{\perp}(n) < 0$ and $0 \leq |\sigma_{\perp}(n)/\tau_{\perp\parallel}(n)| \leq |R^{A}_{\perp\perp}(n)/\tau_{21,c}(n)|$ is calculated according to

$$\frac{1}{S'_{\perp\parallel}(n)}\left(\sqrt{\tau^2_{\perp\parallel}(n) + \left(p^{-}_{\perp\parallel}\sigma_{\perp}(n)\right)^2} + p^{-}_{\perp\parallel}\sigma_{\perp}(n)\right) = f_{e,IFFB}(n) \tag{19}$$

where the fracture resistance $R^{A}_{\perp\perp}(n)$ is calculated by

$$R^{A}_{\perp\perp}(n) = \frac{S'_{\perp\parallel}(n)}{2p^{-}_{\perp\parallel}}\left(\sqrt{1 + 2p^{-}_{\perp\parallel}\frac{Y_c(n)}{S'_{\perp\parallel}(n)}} - 1\right) \tag{20}$$

and the shear stress at the turning point between modus B and C of the failure envelope at $\sigma_{\parallel} = 0$ is defined as

$$\tau_{21,c}(n) = S'_{\perp\parallel}(n)\sqrt{1 + 2p^{-}_{\perp\perp}} \tag{21}$$

where the incline $p^{-}_{\perp\perp}$ is calculated by

$$\frac{p^{-}_{\perp\perp}}{R^{A}_{\perp\perp}(n)} = \frac{p^{-}_{\perp\parallel}}{S'_{\perp\parallel}(n)} \tag{22}$$

The inter fibre failure f_e for Modus C for $\sigma_{\perp}(n) < 0$ and $0 \leq |\tau_{\perp\parallel}(n)/\sigma_{\perp}(n)| \leq |\tau_{21,c}(n)/R^{A}_{\perp\perp}(n)|$) is calculated according to

$$\left[\left(\frac{\tau_{\perp\parallel}(n)}{2\left(1 + p^{-}_{\perp\perp}\right)S'_{\perp\parallel}(n)}\right)^2 + \left(\frac{\sigma_{\perp}(n)}{Y_c(n)}\right)^2\right]\frac{Y_c(n)}{(-\sigma_{\perp}(n))} = f_{e,IFFC}(n) \tag{23}$$

Failure conditions for fibre failure is calculated by

$$\left|\frac{1}{X_{t,c}(n)}\left[\sigma_1(n) - \left(\nu_{\perp\parallel}(n) - \nu_{f\perp\parallel}(n)\frac{E_{\parallel}(n)}{E_{f\parallel}(n)}m_{\sigma f}\right)\sigma_{\perp}(n)\right]\right| = \begin{cases} f_{e,FFT}(n) & \text{with } X_t \text{ for } \sigma_1 \geq 0 \\ f_{e,FFC}(n) & \text{with } X_c \text{ for } \sigma_1 < 0 \end{cases} \tag{24}$$

where $m_{\sigma f}$ is a stress magnification factor, which takes micromechanical effects due to the different moduli of fibre and resin into account. Puck [6] recommends the values $m_{\sigma f} \sim 1.3$ for glass fibre and $m_{\sigma f} \sim 1.1$ for carbon fibre. With $m_{\sigma f} = 1$, $\nu_{f\perp\parallel} = \nu_{\perp\parallel}$ and $E_{f\parallel} = E_{\parallel}$ the simplified fibre failure condition is achieved. In the present paper, the recommendation by Puck is used for all of the investigations. For the downsizing of the failure envelope with endured cycles the parameter $p^{+}_{\perp\parallel}, p^{-}_{\perp\parallel}$ and $p^{+}_{\perp\perp}$ are held constant for simplicity and lack of data. In Figure 10, two shrunken failure envelope af-

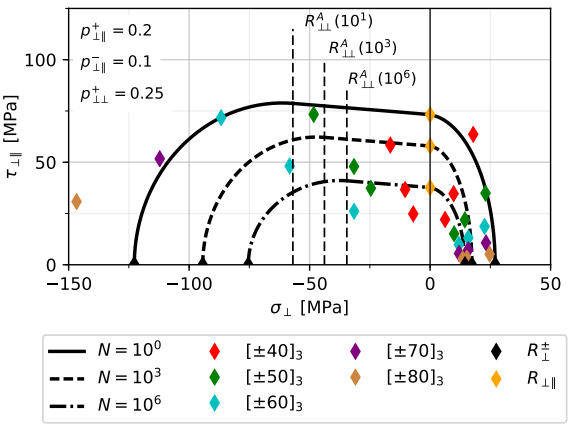

Fig. 10: Comparison of shrunken failure envelopes and experimental data for material D155 [1]

ter different number of endured cycles ($n_1 = 10^3$ and $n_2 = 10^6$) are compared to experimental data of various balanced angle plies from [1]. To plot the results in the $\sigma_{\perp}, \tau_{\perp\parallel}$-plane the data of final laminate failure is

recalculated on the ply level by CLT. Data points of the same color in Fig. 10 represent either residual tensile or residual compression tests of the same laminate lay-up configuration. The data points are obtained from tests at stress ratios R=10 for the compressive transverse stress domain, R=0.1 in the tensile transverse stress domain and R=0.1 for the pure shear shear stress. Only data of laminates, which are mainly affected by transversal and shear stresses ($[\pm 40]_3, ..., [\pm 90]_3$), is projected on the $\sigma_\perp, \tau_{\perp\parallel}$-plane to avoid significant influence of higher fibre-parallel stresses (max. $\sigma_\parallel^+ / R_\parallel^+ \approx 12,5\%$ and max. $\sigma_\parallel^- / R_\parallel^- \approx 17,7\%$ in $[\pm 40]_3$). The fibre volume of used lamina varies between 37% and 40%.

8. Stiffness degradation models

Lots of different models for the stiffness degradation of composite laminates exist in the literature, such as the well known stiffness reduction of graphite/epoxy laminates by Whitworth [35, 36], damage accumulation model by Brondsted et al. [37] or material degradation model used by Shokrieh and Lessard [2]. In the present work Puck's model for the stiffness degradation of perpendicular and shear values due to inter-fibre fracture [38, 39] is preferred in the first instance. The model is used for stiffness degradation in progressive failure analysis in combination with Puck's failure criteria due to static loads, but has already been examined for the modeling under fatigue loads [40].

Knops stated that a degradation of the major Poisson's ratio is not necessary for static calculation [41], [42] and Adden and Horst assumed it for degradation under fatigue as well [40]. Since $\nu_{\perp\parallel}$ stays constant the minor Poisson's ratio $\nu_{\parallel\perp}$ has to be linked to both degraded Young's moduli $E_\perp(n)$ and $E_\parallel(n)$. Since the Young modulus in fibre direction does not decrease very much in early lifecycles, $\nu_{\parallel\perp}$ decreases mainly with chosen values for $E_\perp(n)$. The mechanical properties after each cycle are then derived by the following equations:

$$\begin{bmatrix} E_\perp(n) \\ G_{\perp\parallel}(n) \\ \nu_{\perp\parallel} \\ \nu_{\parallel\perp}(n) \end{bmatrix} = \begin{bmatrix} \eta_\perp(n) \cdot E_{\perp,st} \\ \eta_{\perp\parallel}(n) \cdot G_{\perp\parallel,st} \\ const. \\ \nu_{\perp\parallel} \cdot (E_\perp(n)/E_\parallel(n)) \end{bmatrix} \tag{25}$$

where $\eta_\perp(n)$ and $\eta_{\perp\parallel}(n)$ are calculated for each fracture mode A,B or C separately as recommended for static calculations in [43]. The parameters are derived according to the following equation:

$$\begin{aligned} \eta_\perp(n) &= \frac{1-\eta_{r,\perp}}{1+c_\perp(f_{e,IFF}(n)-1)^{\xi_\perp}} + \eta_{r,\perp} \\ \eta_{\perp\parallel}(n) &= \frac{1-\eta_{r,\perp\parallel}}{1+c_{\perp\parallel}(f_{e,IFF}(n)-1)^{\xi_{\perp\parallel}}} + \eta_{r,\perp\parallel} \end{aligned} \tag{26}$$

In the following the same parameters have been used for degradation after fracture mode A,B or C due to the limited number of experimental data. The assigned values at the ply level are displayed in Figure 11. The degradation of parallel Young's modulus $E_\parallel$ is carried out similar to the residual strength formulation. The main contrast to the procedure in Equation 13 is, that the dependence on the endured number of load cycles is replaced by the actual tensile or compression fibre failure value.

$$E_{\parallel,i+1} = E_{\parallel r,i} - \Delta E_{\parallel r,i} \tag{27}$$

where $E_{\parallel r,i}$ and $E_{\parallel r,i+1}$ are the parallel elastic modulus at the actual and the next step and $\Delta E_{\parallel r,i}$ is the drop in modulus in the ith cycle, which is calculated by the following equation:

$$\Delta E_{\parallel r,i+1} = \left(E_{\parallel,st} - E_{\parallel,f}\left(\sigma_{max}\right)\right) \cdot \left[\left(1-\left(f_{e,i}\right)^{\gamma_i}\right)^{\xi_i} - \left(1-\left(f_{e,i+1}\right)^{\gamma_i}\right)^{\xi_i}\right] \tag{28}$$

Thus the holistic approach is to model all of the stiffness degradation as a function of (inter-)fibre failure, as shown in Fig. 11. Equation 28 provides the same benefits as it does for residual strength calculations. Arbitrary

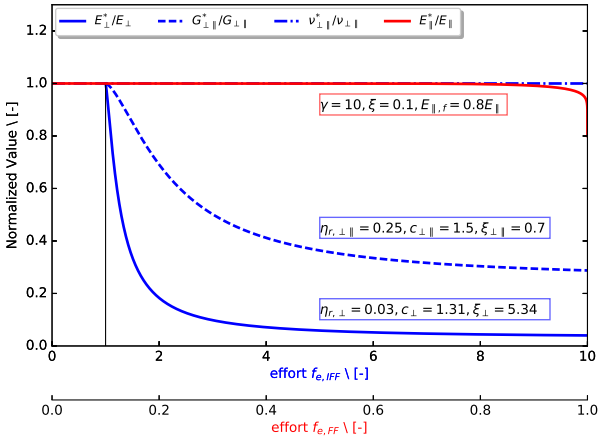

Fig. 11: Application of stiffness degradation models for parallel elastic, transverse elastic and shear moduli.

material behavior with steep drop in stiffness at the beginning as well as sudden drop at the end of life can be modeled.

9. Experimental data

Fatigue data from experimental tests under tension-tension and compression-compression loads are taken from the Composite Material Fatigue Database of the Michigan State University - Department of Energy in cooperation with Sandia National Laboratories (SNL/DOE/MSU - Database) [1]. All of the evaluated coupons were tested at frequencies between 2 and 20 Hz. Each material configuration consists of „Knytex“ e-glass fabrics with varying grammages and a resin system made of orthophthalic polyester (CoRezyn 63-AX-051). The Laminates were fabricated using the Resin Transfer Moulding (RTM) technique: Material #1 - Material #3 is cured at 20°C for 24h and post cured at 60°C for 2h. Material #4 and Material #5 is cured at 20°C for 6h and post cured at 60°C for 2h [1]. The following laminates are chosen to be examined:

9.1. Mat. #1 - Balanced Angle Plies

The first examined material configurations are balanced angle plies, named „D155B, 45D155, 50D155, 60D155, 80D155, 90D155“, with stacking sequences $[0]_5$, $[\pm45]_3$, $[\pm50]_3$, $[\pm60]_3$, $[\pm80]_3$, $[\pm90]_3$, from [1]. The laminates are made from 100 % Knytex e-glass fabrics „D155“ (grammage: $527 g/m^2$), which are orientated to the respective balanced angles. Average volume fraction varies between 37.1 % and 40.4 % and average thickness between 2.70 mm and 3.32 mm.

9.2. Mat. #2 - $[90/0/\pm45/0]_s$

The first examined multi-directional laminate is material „DD16“ from [1], with the laminate stacking sequence: $[90/0/\pm45/0]_s$. It consists of 79 % Knytex e-glass Fabrics „D155“ (grammage: $527 g/m^2$), with 53 % in parallel and 26 % in transverse direction, and of 21 % Knytex e-glass fabrics „DB120 “ (grammage: $393 g/m^2$) orientated in ±45. The average volume fraction is 33.3 % and the average laminate thickness is 4.62 mm.

9.3. Mat. #3 - $[0/\pm45/0]_s$ and $[90/\pm45/90]_s$

Multi-directional laminates „DD5P“ (stacking sequence: $[0/\pm45/0]_s$) and „DD5PT“ (stacking sequence: $[90/\pm45/90]_s$) from [1] consist of 72 % Knytex e-glass fabrics „D155“ in parallel or transverse direction and 28 % Knytex e-glass fabrics „DB120 “ in ±45-direction. Average volume fraction is 37.2 % and average thickness is 3.02 mm.

9.4. Mat. #4 - $[\pm45/0_2/\pm45]_s$

Multi-directional laminate „CH14“ [1] (stacking sequence: $[\pm45/0_2/\pm45]_s$) contains of 39 % Knytex e-glass fabrics „D155“ in parallel direction and 71 % Knytex e-glass fabrics „DB120 “ in ±45-direction. Average volume fraction is 39.2 % and average thickness is 2.49 mm.

9.5. Mat. #5 - $[0/\pm45/0_2/+45]_s$

Multi-directional laminate „CC3“ [1] (stacking sequence: $[0/\pm45/0_2/+45]_s$) contains of 63 % Knytex e-glass Fabrics „D100 “ (grammage: $339 g/m^2$) in parallel direction and 37 % Knytex e-glass fabrics „DB120 “ in ±45-direction. Average volume fraction is 44.4 % and average thickness is 2.74 mm.

10. Results and Discussion

In the first instance, the fatigue life of various balanced angle plies under pulsating tension and pulsating compression stresses is calculated. Fig. 12 shows S-N curves from fitted to experimental data in comparison to the simulated fatigue life data points in logarithmic scale.

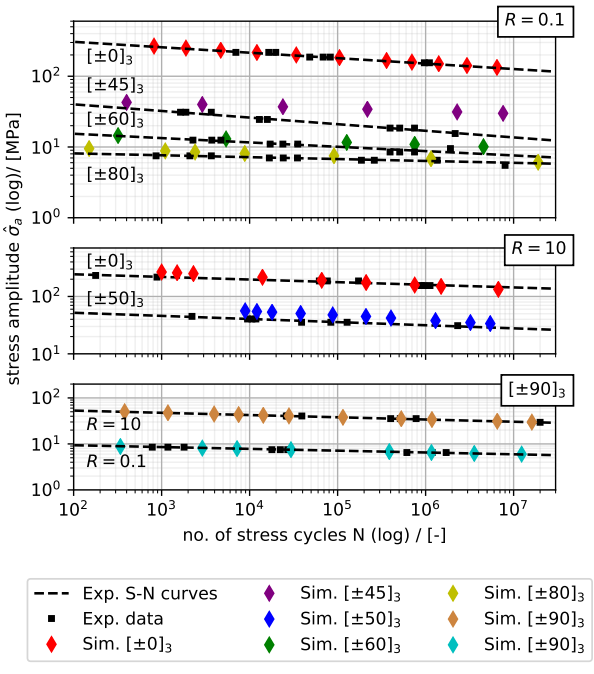

Fig. 12: Lifetime estimation of various angle ply laminates (Mat. #1) under tension-tension (R=0.1) and compression-compression (R=10) fatigue loads compared to experimental data from [1]

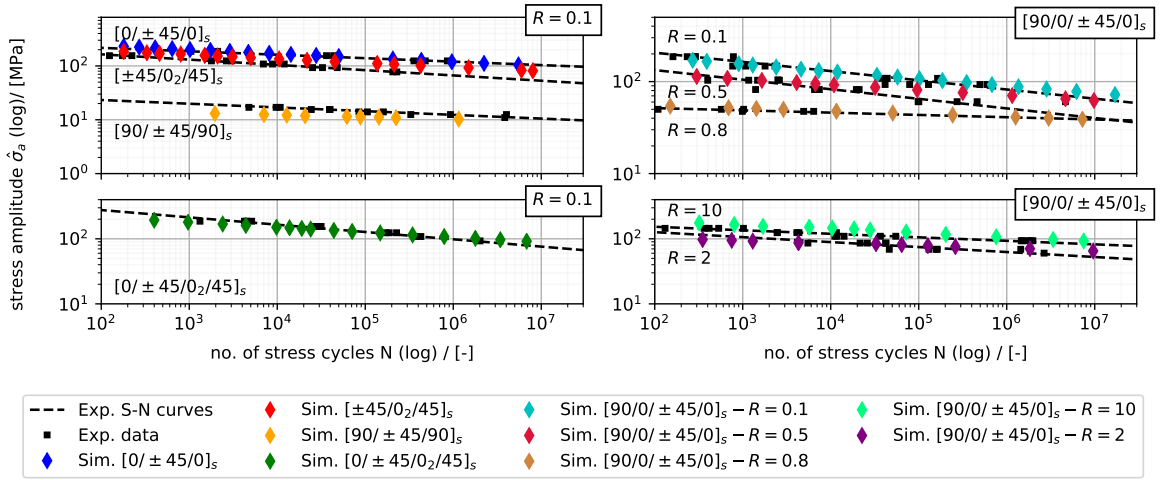

Fig. 13: Lifetime estimation of several multi-directional laminates (Mat. #2 - Mat. #5) under various loading conditions compared to experimental data from [1]

The results for fatigue life estimation of unidirectional material $[\pm0]_3$ and $[\pm90]_3$ are apparently very accurate, under both tension-tension and compression-compression loads, over the whole lifetime period. While results for laminate layups $[\pm50]_3$, $[\pm60]_3$ and $[\pm80]_3$ show very good agreement with the experimental data, the simulation of fatigue life for $[\pm45]_3$ shows substantial, non-conservative deviations in the late-stage. In this context it must be recalled that large deviations appear to be even smaller in logarithmic display. One of the reasons behind this might be the asymmetric CLD of $\tau_{\perp\parallel}$ for the basic material „D155“ (see also S-N curves at $R_{\tau_{\perp\parallel}} = 0.1$ and $R_{\tau_{\perp\parallel}} = 10$ in Fig. 5) and thereby the better fatigue conditions under negative shear stresses. In global T-T loads the $[\pm45]_3$-laminate has the highest local shear load of all the examined balanced angle plies, as can be seen in Fig. 10, and of course fails due to inter fibre failure modus A (following equation 18). While the fracture plane in positive orientated plies (+45°) is calculated from local stress ratios $R_{\sigma_\perp} = 0.1$ and $R_{\tau_{\perp\parallel}} = 10$, in negative orientated plies (−45°) it is calculated with S-N curves at $R_{\sigma_\perp} = 0.1$ and $R_{\tau_{\perp\parallel}} = 0.1$. The higher allowable shear load in those plies definitely makes a difference and leads to higher fatigue life in −45° orientated plies. The effect is reduced with further increasing orientation angle and decreasing local shear loads. This demonstrates how important precise fatigue material tests and formulation of constant life diagrams is within the proposed model. Another main reason for the differences is that, from the author's point of view, the shape of the shrunken failure envelope might change with endured cycles. Considering Fig. 10, the adjustment of failure envelope parameters with the endured number of cycles might deserve further attention. Beside the simulation of $[\pm45]_3$, the model seems to give very satisfactory results for the other balanced angle plies.

In the next step, the fatigue life of various multi-directional laminates is examined. In Fig. 13, the calculated S-N curves are displayed in four different plots for a better overview. Results for Material #3, #4, and #5 for constant amplitude loads at stress ratio R=0.1 are shown in the two left plots. The upper right plot demonstrates the results for Material #2 under three different tension-tension stress ratios (R=0.1, R=0.5 and R=0.8) and the lower right plot shows results for the same material under two compression-compression stress ratios (R=10 and R=2). The model seems to achieve very accurate results for mainly-unidirectional laminates, which mainly consist of fibres aligned in the loading direction (such as Mat. #3 ($[0/\pm45/0]_s$ with 72 % in 0°-direction and Mat. #5 $[0/\pm45/0_2/+45]_s$ with 63 % in 0°-direction). Results for Mat. #3, loaded in the transverse direction ($[90/\pm45/90]_s$), are slightly conservative. Fatigue life calculation for Mat. #4 ($[\pm45/0_2/\pm45]_s$), where 71% fibres are aligned in ±45-direction, is subject to the same effect discussed in the simulation of Mat #1 for $[\pm45]_3$. Fig. 13 apparently shows the growing deviations between calculated and measured fatigue life with increasing number of cycles endured for Mat # 4. It is important to note that the model as well gives results on the non-conservative side for this specific case. Material #2 ($[90/0/\pm45/0]_s$) is examined for different stress ra-

tios in pulsating stress range. Calculations at the border of the tension-tension sector, with R=0.1 (close to R=0), R=0.8 (close to R=1) and R=10 (close to R=∞), show very good agreement with experimental data. The simulation for R=0.5 shows significant discrepancies between calculated and measured data starting from 10^4 cycles. Results at stress ratio R=2 are quite conservative at low cycle fatigue and tend to move to non-conservative predictions at high cycle fatigue. A reason for this is probably the use of only three S-N curves for the basic material. The constant life diagram for Mat. #2, as shown in Fig. 7, seems to confirm this suspicion for the above mentioned stress ratios. Extrapolated data for stress ratio R=0.5 is constantly located in the non-conservative area of the constant life diagram in Fig. 7, but with growing deviations in higher cycles. This agrees with the behavior of simulated data in Fig. 13. Especially the calculated results at stress ratio R=2, in terms of the change from conservative to non-conservative predictions, can be traced back very well to the experimental data in Fig. 7. This clearly shows the importance of constant life diagram formulation within the presented model as well.

Few experimental data for residual strength of laminate #2 is plotted against simulations with varying residual strength parameters at the lamina level in Fig. 14. Four different combinations of parameter $\alpha^+_{i,k}$ and $\beta^+_{i,k}$

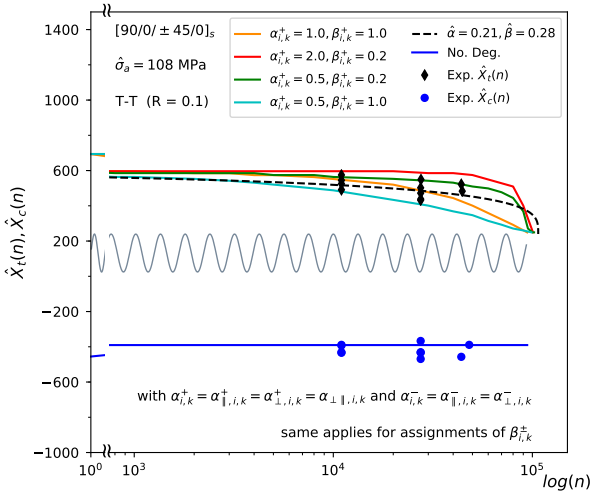

Fig. 14: Comparison of calculated residual strength, for four different combinations of residual strength parameter α^+_i and β^+_i at the lamina-level, with experimental data of residual laminate strength from [1]

are examined, whereby the parameter are the same for every degradation of $R^+_\parallel$, $R^+_\perp$ and $R_{\perp\parallel}$ in each lamina. There is no degradation of compressive strength $R^-_\parallel$ and $R^-_\perp$ modeled for tension-tension loads. The slight decrease in compressive strength at the very beginning is a result of the damaged ±45° and 90° plies. In Fig. 14 the dashed line represents the fitted two-parameter curve from 8 for Material #2. The results indicate that the the two-parameter model by Stojkovic, with parameters $\alpha^+_{i,k} = 0.5$ and $\beta^+_{i,k} = 0.2$, captures the residual strength of the laminate very well over a wide range of load cycles. Even the sudden drop of strength near the end of fatigue life is very accurately displayed. The use of linear strength degradation $\alpha^+_{i,k} = 1$ and $\beta^+_{i,k} = 1$ gives very satisfying results as well, but leads to a steady drop in strength near the end. Both of the other used parameter combinations lead to greatly over- or underestimated results concerning the residual strength. Obviously, all of the examined parameter combinations differ only very little in the calculated fatigue life:

- $N_f(\alpha^+_{i,k} = 1.0 \text{ and } \beta^+_{i,k} = 1.0) = 94200$
- $N_f(\alpha^+_{i,k} = 0.5 \text{ and } \beta^+_{i,k} = 1.0) = 99100$
- $N_f(\alpha^+_{i,k} = 0.5 \text{ and } \beta^+_{i,k} = 0.2) = 102000$
- $N_f(\alpha^+_{i,k} = 2.0 \text{ and } \beta^+_{i,k} = 0.2) = 100700$

This is due to the fact that equation 13 satisfies the fracture condition $\hat{S}_r(n = N) = \sigma_{max}$ in any given case of α^+_i and β^+_i, except of course if no degradation is applied with $\alpha^+_i = 0$. Nonetheless, earlier strength degradation, as for example in linear degradation, leads to slightly earlier inter-fibre failure (equations 18, 19, 23) in some plies and earlier stress redistribution into neighboring plies associated therewith.

In Fig. 15 the calculated residual stiffness of two laminates is compared with experimental data for Material #3. Stacking sequence $[0/\pm45/0]_s$ is tested at stress ratio R=0.1 with amplitude $\hat{\sigma}_a = 124$ MPa and $[90/\pm45/90]_s$ is tested at stress ratio R=0.1 with amplitude $\hat{\sigma}_a = 10.3$ MPa. Data for stiffness degradation from [1] is plotted against calculated data for both laminates in Fig. 15 (a). Stress exposure for failure mode A within the 90° and ±45° orientated plies, as well as stress exposure factor in fibre failure due to tension in the 0° plies, is shown in the central plots (b). In the lower plot the change of the stiffness controlling parameter η_r is plotted (c).

While the calculated initial stiffness of the $[0/\pm45/0]_s$-laminate seems to be greatly overestimated, the calculated stiffness in later cycles is more satisfying. The material behavior is mainly characterized by two key points, numbered as {1} and {2} in the upper plot. In {1}, there is an extremely early drop in stiffness due to premature inter fibre failue in ±45°-orientated plies. The steep increase of the stress exposure factor in $f_{e,IFFA}$ can be

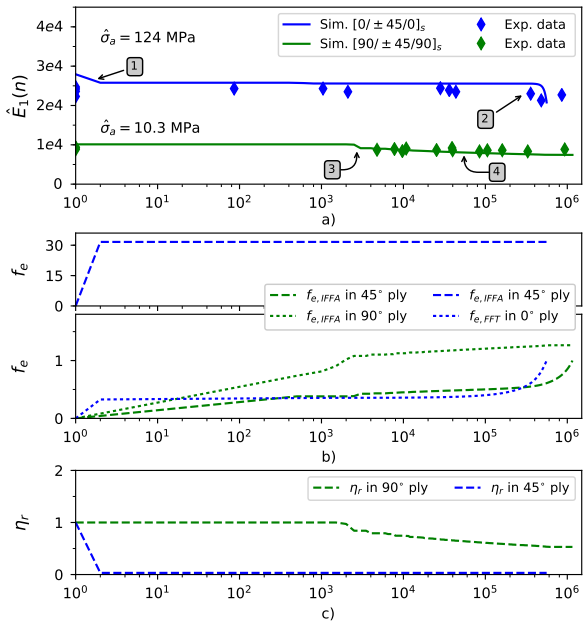

Fig. 15: Comparison of calculated and experimental residual stiffness and for Material #3 from [1]

observed in Fig. 15 (b). Afterwards, the stiffness stays nearly constant over a wide range of cycles until a sudden drop in {2}. This is obviously coupled with the increase of fibre failure, as shown in the central figure. Of course, the behavior at later cycles is strongly dependent on the initial values, which indicates that the differences between calculation and experimental data are mainly caused by the overestimated static stiffness.
Stiffness degradation of the transverse tested Material #3 is calculated considerably better. The static stiffness as well as stiffness at higher cycles is captured very well. The curve is characterized by two main points, numbered as {3} and {4}, too. Due to a steady increase of $f_{e,IFFA}$ in the ±45°-orientated plies at lower cycles, stiffness is decreased after the onset of failure mode A in {3}. Also, in the ±90°-orientated plies, there is a rapid rise in fibre failure in {3} due to stress redistribution. Afterwards, there is a continuous decrease in laminate stiffness until global failure in {4}.

11. Conclusions and future work

After a brief review of literature, a model for fatigue life analysis is introduced, which is characterized by its iterative and progressive procedure for the calculation of the current laminate conditions at every load cycle. Different sectors and models applied within the methodology are described in detail. Afterwards, various multi-directional fibre reinforced plastic laminates are calculated and presented. Fatigue life for several balanced angle ply laminates under pulsating tension and compression loads is calculated and compared to experimental data. A quantity of multi-directional laminates with arbitrary stacking sequences under different stress ratios are examined and verified, too. Furthermore, residual strength and stiffness of different laminates are considered in more detail. Altogether, the predictions of the model showed a good correlation with most of the experimental data. Any discrepancies or unusual material behaviors are traced back to certain input parameters or known issues, which will be addressed in future work. To sum up, the model tends to be capable of simulating fatigue life of multi-directional laminates under complex multiaxial loads with different stress ratios accurately.
Still the findings leave questions for the future, which will be addressed in forthcoming works:

- As it is crucial to know the laminates capacity of carrying further loads after a certain time period, a more in-depth analysis of residual strengths models and their application within the model will be carried out next. Detailed strength degradation after certain combined loads, particularly in multiaxially loaded multi-directional laminates, will be addressed.

- As the investigations in the present paper have shown, a deeper look on the failure envelope for multiaxial fatigue might be an advantage for further simulations of fatigue life. For deeper investigations of off-axis plies, failure envelope characteristics after certain number endured cycles will also be addressed.

- Since the shape of the failure envelope changes significantly with the used boundary conditions in terms of S-N curves of $R_{\perp}^{+}$, $R_{\perp}^{-}$ and $R_{\perp\parallel}$ at varying stress ratios, the influence of non-proportional loads will be taken into consideration in future works.

References

[1] J. Mandell, D. Samborsky, SNL/MSU/DOE composite materials fatigue database V22.0, U.S. Department of Energy, Sandia National Laboratories, Montana State University, Bozeman, Montana, 2014.

[2] M. Shokrieh, L. Lessard, Progressive fatigue damage modeling of composite materials, part i: Modeling, Journal of Composite Materials 34 (2000) 145–159. doi:DOI:10.1177/002199830003401301.

[3] Z. Hashin, Fatigue failure criteria for combined cyclic stress, International Journal of Fracture 17 (2) (1981) 101–109. doi:10.1007/BF00053514.
URL https://doi.org/10.1007/BF00053514

[4] M. Shokrieh, L. Lessard, Progressive fatigue damage modeling of composite materials, part ii: Material characterization and model verification, Journal of Composite Materials 34. doi:https://doi.org/10.1177/002199830003401302.

[5] T. Noll, M. Magin, N. Himmel, Fatigue life simulation of multiaxial cfrp laminates considering material non-linearity, International Journal of Fatigue 32 (1) (2010) 146 – 157, fourth International Conference on Fatigue of Composites (ICFC4). doi:https://doi.org/10.1016/j.ijfatigue.2009.02.019.
URL http://www.sciencedirect.com/science/article/pii/S014211230900067X

[6] A. Puck, H. Schürmann, Failure analysis of frp laminates by means of physically based phenomenological models, Composites Science and Technology 62 (12) (2002) 1633 – 1662. doi:https://doi.org/10.1016/S0266-3538(01)00208-1.
URL http://www.sciencedirect.com/science/article/pii/S0266353801002081

[7] C. Kennedy, C. Bradaigh, S. Leen, A multiaxial fatigue damage model for fibre reinforced polymer composites, Composite Structures 106 (2013) 201–210. doi:http://dx.doi.org/10.1016/j.compstruct.2013.05.024.

[8] H. Mao, S. Mahadevan, Fatigue damage modelling of composite materials, Composite Structures 58 (4) (2002) 405 – 410. doi:https://doi.org/10.1016/S0263-8223(02)00126-5.
URL http://www.sciencedirect.com/science/article/pii/S0263822302001265

[9] M. Neumeister, M. Wagner, I. Becker, M. Decker, Potenziale im zusammenspiel von versuch und berechnung in der betriebsfestigkeit, Deutscher Verband für Materialforschung und -prüfung e.V. 43. Tagung des DVM-Arbeitskreises Betriebsfestigkeit (2016) 243 – 259.
URL https://www.iabg.de/fileadmin/media/Geschaeftsfelder/Automotive/PDF/Neumeister_et_al_-_Betriebsfestigkeit_Faserverbunde_-_FatiLaminate__DVM_2016_.pdf

[10] R. Cuntze, A. Freund, The predictive capability of failure mode concept-based strength criteria for multidirectional laminates, Composites Science and Technology 64 (3) (2004) 343 – 377, failure criteria in fibre reinforced polymer composites Part C: Additional theories conclusions and recommendations. doi:https://doi.org/10.1016/S0266-3538(03)00218-5.
URL http://www.sciencedirect.com/science/article/pii/S0266353803002185

[11] M. Shokrieh, L. Lessard, 3 - fatigue under multiaxial stress systems, in: B. Harris (Ed.), Fatigue in Composites, Woodhead Publishing Series in Composites Science and Engineering, Woodhead Publishing, 2003, pp. 63 – 113. doi:https://doi.org/10.1533/9781855738577.1.63.
URL https://www.sciencedirect.com/science/article/pii/B9781855736085500085

[12] V. G. Mejlej, D. Osorio, T. Vietor, An improved fatigue failure model for multidirectional fiber-reinforced composite laminates under any stress ratios of cyclic loading, Procedia CIRP 66 (Supplement C) (2017) 27 – 32, 1st CIRP Conference on Composite Materials Parts Manufacturing (CIRP CCMPM 2017). doi:https://doi.org/10.1016/j.procir.2017.03.303.
URL http://www.sciencedirect.com/science/article/pii/S2212827117304912

[13] M. Shokrieh, F. Taheri-Behrooz, A unified fatigue life model based on energy method, Composite Structures 75 (1) (2006) 444 – 450, thirteenth International Conference on Composite Structures. doi:https://doi.org/10.1016/j.compstruct.2006.04.041.
URL http://www.sciencedirect.com/science/article/pii/S026382230600170X

[14] R. S. Sandhu, R. L. Gallo, G. P. Sendeckyj, Initiation and accumulation of damage in composite laminates, Composite Materials (1982) 163–182Testing and Design (Sixth Conference), ASTM STP 787, American Society for Testing and Materials.

[15] A. P. Vassilopoulos, R. Sarfaraz, B. D. Manshadi, T. Keller, A computational tool for the life prediction of gfrp laminates under irregular complex stress states: Influence of the fatigue failure criterion, Computational Materials Science 49 (3) (2010) 483 – 491. doi:https://doi.org/10.1016/j.commatsci.2010.05.039.
URL http://www.sciencedirect.com/science/article/pii/S0927025610003113

[16] Z. Fawaz, F. Ellyin, Fatigue failure model for fibre-reinforced materials under general loading conditions, Journal of Composite Materials - J COMPOS MATER 28 (1994) 1432–1451.

[17] Z. Hashin, A. Rotem, A fatigue failure criterion for fiber reinforced materials, Journal of Composite Materials - J COMPOS MATER 7 (1973) 448–464.

[18] G. Sendeckyj, Constant life diagrams âĂŤ a historical review, International Journal of Fatigue 23 (4) (2001) 347 – 353. doi:https://doi.org/10.1016/S0142-1123(00)00077-3.
URL http://www.sciencedirect.com/science/article/pii/S0142112300000773

[19] A. Vassilopoulos, B. Manshadi, T. Keller, Influence of the constant life diagram formulation on the fatigue life prediction of composite materials, International Journal of Fatigue 32 (2010) 659–669. doi:https://doi.org/10.1016/j.ijfatigue.2009.09.008.

[20] G. Lloyd, Guideline for the Certification of Wind Turbines, Germanischer Lloyd Industrial Services GmbH, Renewables Certification, Hamburg, Germany, 2010.

[21] M. Kawai, M. Koizumi, Nonlinear constant fatigue life diagrams for carbon/epoxy laminates at room temperature, Composites Part A: Applied Science and Manufacturing 38 (11) (2007) 2342 – 2353, compTest 2006. doi:https://doi.org/10.1016/j.compositesa.2007.01.016.
URL http://www.sciencedirect.com/science/article/pii/S1359835X07000231

[22] B. Harris, A parametric constant-life model for prediction of the fatigue lives of fibre-reinforced plastics, Fatigue in Composites: Science and Technology of the Fatigue Response of Fibre-Reinforced Plastics (2003) 546–568.

[23] G. Boerstra, The multislope model: A new description for the fatigue strength of glass fibre reinforced plastic, International Journal of Fatigue 29 (8) (2007) 1571 – 1576. doi:https://doi.org/10.1016/j.ijfatigue.2006.11.007.
URL http://www.sciencedirect.com/science/article/pii/S0142112306003264

[24] T. P. Philippidis, A. P. Vassilopoulos, Life prediction methodology for gfrp laminates under spectrum loading, Composites Part A: Applied Science and Manufacturing 35 (6) (2004) 657 – 666. doi:https://doi.org/10.1016/j.compositesa.2004.02.009.
URL http://www.sciencedirect.com/science/article/pii/S1359835X04000466

[25] A. P. Vassilopoulos, B. D. Manshadi, T. Keller, Piecewise non-linear constant life diagram formulation for frp composite materials, International Journal of Fatigue 32 (10) (2010) 1731 – 1738. doi:https://doi.org/10.1016/j.ijfatigue.2010.03.013.
URL http://www.sciencedirect.com/science/

article/pii/S0142112310000794

[26] T. Philippidis, V. Passipoularidis, Residual strength after fatigue in composites: Theory vs. experiment, International Journal of Fatigue 29 (12) (2007) 2104 – 2116. doi:https://doi.org/10.1016/j.ijfatigue.2007.01.019.
URL http://www.sciencedirect.com/science/article/pii/S0142112307000369

[27] L. Broutman, S. Sahu, A new theory to predict cumulative fatigue damage in fiberglass reinforced plastics, Composite Materials: Testing and Design (2nd Conference), ASTM STP497, Corten HT (1972) 170–188doi:10.1520/STP27746S.

[28] J. R. Schaff, B. D. Davidson, Life prediction methodology for composite structures. part iŮconstant amplitude and two-stress level fatigue, Journal of Composite Materials (1997) 170–188doi:10.1177/002199839703100202.

[29] N. Stojkovic, F. Radomir, H. Pasternak, Mathematical model for the prediction of strength degradation of composites subjected to constant amplitude fatigue, International Journal of Fatigue 103 (2017) 478–487. doi:https://doi.org/10.1016/j.ijfatigue.2017.06.032.

[30] J. Wang, B. Karihaloo, Optimum in situ strength design of composite laminates. part i: in situ strength parameters, Journal of Composite Materials (1996) 1314–1337doi:10.1177/002199839603001202.

[31] H. Dong, Z. Li, J. Wang, B. Karihaloo, A new fatigue failure theory for multidirectional fiber-reinforced composite laminates with arbitrary stacking sequence, International Journal of Fatigue 87 (2016) 294–300. doi:https://doi.org/10.1016/j.ijfatigue.2016.02.012.

[32] M. Hinton, A. Kaddour, P. Soden, Failure Criteria in Fibre reinforced polymer composites: The World-Wide Failure Exercise. A Composites Science and Technology Compendium, Elsevier Ltd., UK, 2004.

[33] A. S. Kaddour, M. Hinton, P. D Soden, A comparative study of failure theories and predictions for fibre polymer composite laminates: Part (a) (2004) 664–701.

[34] A. S. Kaddour, M. Hinton, P. D Soden, Predictive capabilities of nineteen failure theories and design methodologies for polymer composite laminates. part b: Comparison with experiments (2004) 1073–1221.

[35] H. Whitworth, Modeling stiffness reduction of graphite/epoxy composite laminates, Journal of Composite Materials - J COMPOS MATER 21 (1987) 362–372.

[36] H. Whitworth, A stiffness degradation model for composite laminates under fatigue loading, Composite Structures 40 (2) (1997) 95 – 101. doi:https://doi.org/10.1016/S0263-8223(97)00142-6.
URL http://www.sciencedirect.com/science/article/pii/S0263822397001426

[37] P. Brøndsted, S. Andersen, H. Lilholt, Fatigue damage accumulation and lifetime prediction of GFRP materials under block loading and stochastic loading, Risø National Laboratory, 1997, pp. 269–278.

[38] A. Puck, Festigkeitsanalyse von Faser-Matrix-Laminaten - Modelle für die Praxis, Carl Hanser Verlag, München ; Wien, 1996.

[39] A. Puck, M. Mannigel, Physically based non-linear stress-strain relations for the inter-fibre fracture analysis of frp laminates, Composites Science and Technology 67 (9) (2007) 1955 – 1964. doi:https://doi.org/10.1016/j.compscitech.2006.10.008.
URL http://www.sciencedirect.com/science/article/pii/S0266353806003952

[40] S. Adden, P. Horst, Stiffness degradation under fatigue in multiaxially loaded non-crimped-fabrics, International Journal of Fatigue 32 (2010) 108–122. doi:https://doi.org/10.1016/j.ijfatigue.2009.02.002.

[41] M. Knops, Sukzessives Bruchgeschehen in Faserverbundlaminaten Gradual failure process in fibre/polymer laminates, Vol. IKV Aachen, Band 140, Verlag Mainz, Aachen, Diss., 2003.

[42] M. Knops, C. Bögle, Gradual failure in fibre/polymer laminates, Composites Science and Technology 66 (2005) 616–625. doi:https://doi.org/10.1016/j.compscitech.2005.07.044.

[43] H. Schürmann, Konstruieren mit Faser-Kunststoff-Verbunden, Springer-Verlag, Berlin ; Heidelberg, 2007.

Mobility and Engineering Research (MER)
Volume 1/2018

Impressum

This document is published within the series 'Mobility and Engineering Research (MER)'.
All publications can be downloaded from https://cos.bibl.th-koeln.de/home.

Date of publication: August, 2018

Editorship of Series

Contact editor's office

Prof. Dr. Jochen Blaurock
TH Köln
Faculty of Automotive Systems and Production
Institute for Automotive Engineering
Betzdorfer Straße 2
50679 Köln
phone: +49 221-8275-2890
email: jochen.blaurock@th-koeln.de

Technology
Arts Sciences
TH Köln